Multifunctional ferrite-albumin nanopaticles in nanomedicine

Magnetic nanoparticles attract wide attention in modern medicine and pharmacology owing to their potential usefulness as contrast agents in magnetic resonance imaging, magnetic carriers for drug targeting and heat generator mediators in hyperthermia treatment. Many different methods are used for their synthesis but, often, the approaches adopted do not permit to obtain nanoparticles with the properties required for biomedical applications. In this work, nanoparticles with a narrow size distribution and an elevated fraction of the magnetic component (about 40 wt%) were obtained by synthesizing and entrapping superparamagnetic manganese ferrite in an albumin matrix. For the purpose reverse micelle systems were used as synthesizing media both for precipitation of inorganic nanoparticles and polymeric coating. After physico-chemical characterization a model drug was loaded on the nanocomposite powder and the biological activity of the nanotechnological system was evaluated

Mariangela Bellusci, Aurelio La Barbera, Franco Padella, Daniela Secci

Nanoparticelle multifunzionali a base di ferrite-albumina in nanomedicina

Le nanoparticelle magnetiche hanno attratto l'attenzione della medicina moderna e della farmacologia grazie alle loro potenziali applicazioni come agenti di contrasto nella risonanza magnetica, come veicolanti di farmaci su siti specifici e come mediatori per lo sviluppo di calore nell'ipertermia. La sintesi di tali sistemi può essere realizzata mediante diversi metodi ma, spesso, gli approcci utilizzati non permettono di ottenere nanoparticelle aventi le proprietà necessarie per un'applicazione biomedica. In questo lavoro, nanoparticelle aventi una stretta distribuzione dimensionale ed un elevato contenuto di componente magnetica (circa 40% in peso) sono state sviluppate mediante sintesi e intrappolamento in albumina di ferrite di manganese superparamagnetica. A tale scopo sono stati utilizzati sistemi di micelle inverse quali nanoreattori di sintesi sia per la precipitazione delle nanoparticelle inorganiche che per il successivo coating polimerico. Dopo la caratterizzazione chimico-fisica dei sistemi sviluppati un farmaco modello è stato caricato sul nanocomposito e ne è stata valutata la sua attività biologica

Mariangela Bellusci, Aurelio La Barbera, Franco Padella
ENEA, Unità Tecnica Tecnologia dei Materiali, Laboratorio di Chimica e Tecnologia dei materiali
Daniela Secci
Università degli Studi di Roma "La Sapienza", Dipartimento di Studi di Chimica e Tecnologia delle Sostanze Biologicamente Attive

INTRODUCTION

Theranostic nanomedicine, defined as an integrated nanotherapeutic system which can diagnose, deliver targeted therapy and monitor the response to therapy, is an important ongoing challenge of future medicine and cancer treatment.

A successful development of theranostic nanomedicine requires significant S&T advances of nanostructured and nanocomposite materials. Ideal nanomaterials should be non-toxic, small in size, provide high drug-loading, be efficient in targeting with minimal nonspecific uptake, improving responsive release of the therapeutic agent with ultra-sensitive imaging.

Magnetic mixed metal-oxide nanoparticles and, in particular, superparamagnetic iron-oxide nanoparticles (SPION), that are the only clinically FDA approved metal oxide nanoparticles, have a crucial role in developing theranostic nanomedicine [1-11]. These particles, in fact, in superparamagnetic conditions and in the form of injectable stable suspensions (ferrofluids) can be driven and fixed to a target site by an external magnetic field thus allowing site-specific drug release. Moreover, magnetically-driven or by antibody conjugation mediation, nanoparticles can selectively deposit heat to a target site (hyperthermia) through an alternating magnetic field. Finally, superparamagnetic nanoparticles can be used as contrast agents in magnetic resonance imaging [6, 7], due to their effects on proton relaxation time.

The superparamagnetic property is strictly required for these applications.

Superparamagnetism is a property that a nanoparticle assembly can show when the powder is below a critical nanometric size for a given chemical composition. Superparamagnetic particles consist of a single magnetic domain with a magnetization behaviour similar to that of atomic paramagnets, except that they have higher magnetic susceptibility values. Hence they do not exhibit residual magnetization when the external field is removed. The absence of residual magnetization avoids unwanted agglomeration phenomena and then the possible embolization of capillary vessels.

Superparamagnetic nanoparticles in powder and suspension forms are already commercially available, yet in-house synthesis is necessary to design, engineer and control the material for its specific application.

In the work reported in this paper, with the aim of obtaining a biocompatible system having a narrow size distribution and an elevated fraction of magnetic component, superparamagnetic manganese ferrite ($MnFe_2O_4$) nanoparticles were synthesized and entrapped into an albumin matrix. The powder so obtained, showing a narrow size distribution, was characterized in terms of its physicochemical properties. Finally, focusing the attention on treatments of medical device-related infections, an antibiotic was linked to the nanocomposite and the biological activity was tested.

EXPERIMENTAL

$MnFe_2O_4$ particles synthesis and treatments

Manganese ferrite nanoparticles were obtained by coprecipitation from Fe^{3+} and Mn^{2+}, in a water-in-toluene micellar system. A 0.4 M solution of the surfactant agent, sodium dodecylbenzenesulfonate (NaDBS, from Aldrich, technical grade) was prepared by solving an appropriate quantity of the organic salt in water. The solution starting metallic salts (0.4 M in Fe^{3+} and 0.2 M in Mn^{2+}) was prepared by dissolving $Fe(NO_3)_3 \cdot 9H_2O$ (Riedel-de Haël, ACS grade) and $Mn(NO_3)_2 \cdot 4H_2O$ (Fluka, purity ≥ 97%) in water. A volume of the metal ions solution was mixed with an equivalent volume of the surfactant solution and a toluene excess. The obtained liquid mixture was stabilized in a microemulsion phase by a prolonged stirring action (24h).

A 1M NaOH aqueous solution, in stoichiometric quantity to produce $MnFe_2O_4$ from metal ions, was added to the microemulsion so that the final water to toluene volume ratio was 1:20. The suspension obtained was stirred for 2 h. To avoid Mn^{2+} oxidation, degassed solvents were utilised and nitrogen atmosphere was applied. The powder suspension was digested under inert gas flow, by keeping it at 100 °C for 90 minutes. The precipitated phase was collected by centrifugation and successively washed with 1:1 water/ethanol solution that acts as a solvent mixture for the surfactant. After vacuum drying (40 °C), a fine dark brown powder was obtained (the sample is called D90m hereafter). The sample was heated at 600 °C (C600 hereafter), selecting the temperature on the basis of the sample thermogravimetric analysis [12].

Nanocomposite preparation

Manganese ferrite nanoparticles (C600 sample) were entrapped into an albumin matrix (Bovine Serum Albumine, BSA hereafter) by cross-linking albumin with glutaraldehyde inside an emulsion system. The emulsion consisted of the water/cyclohexane/sorbitan monoleate system optimized for BSA nanoparticles preparation. In detail, surfactant concentration was fixed at 5% (w/w), BSA concentration at 5% (w/w), glutaraldehyde at 25% (w/w), water to oil ratio at 1/10 (v/v); the mixture was then stirred by using a homogenizer at 22000 rpm.

Figure 1 reports a schematic representation of nanocomposite preparation.

In the first step of the developed preparation route, in order to obtain hydrophilized ferrite nanoparticles, a dispersion of ferrite in an albumin aqueous solution was prepared by using a 1:4 w/w ferrite/albumin ratio (as shown in Figure 1). The mixture was sonicated for 1 h, in nitrogen atmosphere to avoid manganese ferrite oxidation, and then kept for 1 h in static condition.

In the second step, the hydrophilic dispersion was emulsified with a cyclohexane solution of sorbitan monoleate. After mixing for 1 min, BSA cross-linking was started by adding glutaraldehyde dropwise and the suspension was stirred for 2 min [13].

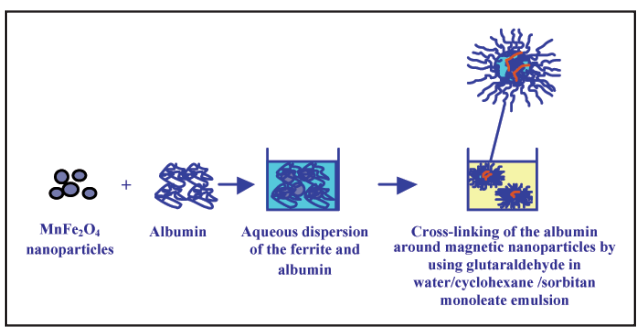

FIGURE 1 Schematic representation of nanocomposite preparation
Source: ENEA

Physico-chemical characterizations

The obtained materials were analysed in order to establish their chemical composition. The residue content of the organic surfactant utilised in the synthesis process of the manganese ferrite and the organic content in nanocomposite were estimated from elemental analysis (Carlo Erba EA 1110 C H N S apparatus).

The metal content (Fe/Mn ratio) was determined by Inductively Coupled Plasma - Optical Emission Spectroscopy (ICP-OES) (Varian Vista MPX CCD apparatus) solubilising the powders in hydrochloric acid.

Thermogravimetric analysis and thermal treatments were performed under inert gas flux (Ar, 100cc/min) by using a Perkin-Elmer Pyris Diamond TGA/DTA, coupled to a Quadrupole Spectrometer (Balzer) to analyse gas evolution.

Differential scanning calorimetry (DSC) analysis was carried out by using a METTLER TA 3000 calorimeter equipped with a TC 10A processor.

IR spectroscopy was performed in transmission mode by employing a Fourier Transformed IR (FT-IR) Mattson Galaxy 5000 spectrometer; data elaboration was performed using the FIRST Software. Samples were prepared in KBr tablets by employing a CARVER Laboratory Press.

X-ray diffraction methods were utilised to investigate the phase content in the synthesized oxide powder and in nanocomposite preparation. A Siemens D500 apparatus (Mo K_{a1} radiation) was utilised for the purpose. Qualitative results were obtained by comparison, using the JCPDS-ICDD database [14]. Doubtful attributions were resolved by evaluating peaks intensities and profiles, using XFIT [15] profile minimisation program, and applying a semi-quantitative comparison method. Quantitative phase analyses of the examined powders were obtained by Rietveld method [16], using GSAS [17] program and structural models obtained from the ICSD 2004 database [18].

Transmission electron microscopy (TEM) images were acquired in dark and bright field mode using a JEOL 200 CX. Samples were prepared by dispersing the powder in isooctane and deposing a drop of the suspension on a copper grid, coated with amorphous carbon material.

Scanning electron microscopy (SEM) images were acquired by using a HRSEM LEO 130. The average particle size was evaluated by using the IMAGE J 1.36 b program.

The magnetic properties of the $MnFe_2O_4$ spinel ferrite were characterized by Superconducting Quantum Interference Device (SQUID) (MPMS 5 Quantum Design).

Material functionalization with bioactive molecules

Cefamandole nafate (CEF, Eli Lilly ITALIA) was adsorbed on the composite nanoparticles.

For the antibiotic adsorption, 0.06 grams of composite nanoparticles were first introduced into a SpectaPor cellulose dialysis tube, with a molecular weight cutoff (12000-14000 Dalton) which prevented nanoparticles diffusion, and then put in contact for 24 h with a 0.04 M antibiotic solution at room temperature. After antibiotic adsorption, nanoparticles were washed with water for 2 h to remove excess unbound antibiotic. The obtained systems were called $MnFe_2O_4$-BSAn-CEF_{ads}.

The amount of adsorbed cefamandole was evaluated by UV-VIS spectroscopy by checking the absorbance of the antibiotic solution at 270 nm before and after the contact with the nanoparticles, and by comparing it with a standard curve (absorbance vs. concentration).

The kinetics of antibiotic release was studied by keeping the nanoparticles in saline solution for increasing times. The aqueous solution was then sampled hourly for the first 5 - 6 hours and at 24 hr intervals, and then analyzed by UV spectroscopy for the evaluation of cefamandole content.

Microbiological tests

Staphylococcus epidermidis, strain ATCC 35984, was employed in the experiments and the cefamandole nafate minimum inhibitory concentration (MIC) in agar medium against this strain was 0.2 g/ml. For assessment of nanoparticle antimicrobial activity by turbidimetric analysis, two tubes were filled with 2 ml Muller Hinton (MH, Oxoid) broth; one tube was used as reference (control) while 0.06 grams of cefamandole-treated nanoparticles were added in the other tube (test). Tubes were inoculated with a 10^8 CFU/ml bacterial solution at the logarithmic phase of growth and incubated overnight at 37 °C. Following incubation, the absorbance at 550 nm of each test solution was measured and compared with that of the control tube. Since the amount of adsorbed light increases with an increase in cell population, the lack of activity of the antibiotic-treated nanoparticles was correlated to an increase in the absorbance of the test tube solution.

Cytotoxicity assay

For material cytotoxicity assay, human larynx carcinoma (Hep-2) cells were grown as monolayers in Minimum Essential Medium (MEM) supplemented with 10% Fetal Bovine Serum (FBS), 1% non-essential amino acids, 5mM L-glutamine, 1% penicillin/streptomycin in a humidified atmosphere with 5% CO_2 at 37°C. Cells were plated on glass coverslips in 24-well plates (inoculum of 5×10^3 cells/ml) and were grown for 24 h either in absence (control) or in presence of 0.06 g of nanoparticles. Following 24 h incubation, cells were fixed with 3.7% formaldehyde solution in phosphate buffer (PBS, pH = 7.4) for 10 min at room temperature, washed in PBS and permeabilised with a 0.5% Triton X-100 (Sigma) solution in PBS for 10 min at room temperature. For F-actin detection, cells were stained with fluorescein isothiocyanate-phalloidin (Sigma) and incubated at 37°C for 30 min. Following staining, cells were washed in PBS, mounted in glycerol-PBS (2:1) and analysed with a Nikon Optiphot fluorescence microscope.

RESULTS AND DISCUSSION

Synthesis of the magnetic component

The chemical analysis of the examined samples is reported in Table 1. As expected, the Fe/Mn ratio is very close to 2. Excluding the sample treated at 600 °C, the organic residues, arising from the micellar system, were present in quantities around 2 wt%.

TABLE 1 Chemical analysis

Sample	Fe/Mn	NaDBS Weight (%)
D90m	1.95±0.05	1.9±0.1
C600	1.95±0.05	<0.3*

* elemental carbon content

Source: ENEA

Figure 2 reports XRD patterns for all the obtained powders. D90m sample produces diffrattograms consisting of sequences of irregular haloes, as a consequence of broad peaks overlapping due to the poorly structured characteristics of the precipitated sample. Well defined indications of manganese ferrite phase occurrence were not observed.

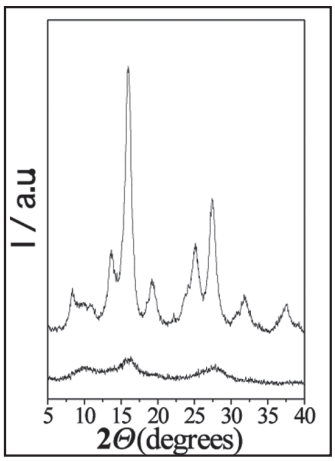

FIGURE 2
X-ray diffraction patterns resulting from D90m sample before (lower curve) and after 600 °C (upper curve) thermal treatment
Source: ENEA

At higher temperatures the XRD pattern clearly evolves toward the expected one. In fact, the sample calcined at 600 °C shows the X-ray pattern of $MnFe_2O_4$ spinel ferrite.
The results of qualitative and quantitative phase analysis, as well as estimations of the mean crystallite sizes of the constituents are reported in Table 2.
The samples precipitated and digested 90min at 100 °C consist in oxo-hydroxide phases. To achieve ferrite nucleation, a calcination process at elevated temperature was then required.

TABLE 2 Quantitative phase analysis

Phase	D90m		C600	
	Wt (%)	<D> (nm)	Wt (%)	<D> (nm)
$(Fe_{2/3}Mn_{1/3})(OH)_{8/3}$ *22-0346 [a]	77	1._4		
$(Fe_{2/3}Mn_{1/3})O_{2/3}(OH)_{4/3}$ *79-0416 [b]	23	1._4		
$MnFe_2O_4$ *10-0319			79	4._8
$(FeMn)O_3$ [19] *83-0112			14	10._1
Fe_2O_3 *33-0664			7	10._1

*JCPDS-ICDD database card – [a]$Fe(OH)_3$ phase type [20]; [b]Fe_3O_4 phase type
Source: ENEA

Representative TEM images of the powders are reported in Figure 3. Although the particles were dispersed with the aid of a sonicator, a strong agglomeration tendency due to interparticle interactions is shown. Powder samples are constituted by agglomerates of nanocrystallites with average size of ~2 nm in case of D90m sample, about 5 nm in case of C600.

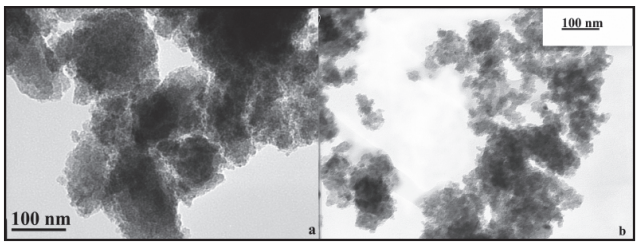

FIGURE 3 Representative TEM of (a) D90m and (b) C600 samples
Source: ENEA

Entrapment of the $MnFe_2O_4$ nanoparticles in albumin and physico-chemical characterization

Engineering surfaces of synthesized nanoparticles by organic molecules has different tasks to fulfil: (i) to stabilize the nanoparticles in a biological suspension, (ii) to provide functional groups at the surface for further derivatization, and, finally, (iii) to improve material biocompatibility.
The developed magnetic nanocomposites may typically have the two structural configurations reported in Figure 4: a magnetic particle core coated with biocompatible polymer or porous biocompatible polymer containing inside magnetic nanoparticles.
Surfactant-assisted synthesis is an interesting approach to develop ceramic-polymer composites. This method still shows some imperfections such as: small amounts and heterogeneous distribution of magnetic nanoparticles that can be loaded inside each particle.

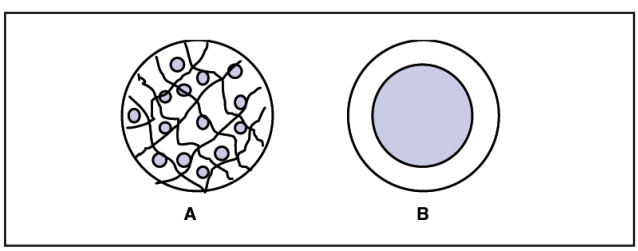

FIGURE 4 Coating type (A) nanoparticle entrapment, (B) core-shell structure
Source: ENEA

In order to guarantee large dispersion of magnetic particles into the polymer we carried out the direct dispersion of the magnetic particles into the polymer of interest followed by emulsification and, finally, polymer cross-linking.

The qualitative phase composition of the nanocomposite was investigated by IR and XRD analysis.

Figure 4 shows the FTIR spectra for $MnFe_2O_4$, pure BSA, GLA-crosslinked BSA and $MnFe_2O_4$-BSA.

The $MnFe_2O_4$ spectrum shows characteristic peaks in ranges 400–580 cm^{-1} (M–O stretching) and 700–1100 cm^{-1} (M–OH and M–OH_2 stretching) [19]. The band in range 1340–1650 cm^{-1} is characteristic for H–O–H bending and corresponds to molecular water adsorbed or incorporated into the crystalline lattice [20]. The broad band in range 2500–3650 cm^{-1} corresponds to symmetric and asymmetric stretching of the O–H bond. The presence of M–OH and M–OH_2 groups is characteristic of water sorption on oxide, particularly enhanced in the case of the nanoparticles. The BSA spectrum exhibits characteristic absorptions at 1634, 1528 and 1451 cm^{-1} due to amide I, amide II and amide III bands, respectively. Absorption bands at 1075 cm^{-1} and in range 666–800 cm^{-1} are attributed to C–N stretching and to out-of plane N–H wagging. Other features are amidic stretching centred at 3300 cm^{-1}, carboxylic O–H stretching centred at 3200 cm^{-1} and symmetric and asymmetric stretching of NH^{3+} groups in range 2800–2900 cm^{-1}. Crosslinking of BSA involves an alteration of the intensity ratios of bands characteristic for pure albumin. The spectrum of the $MnFe_2O_4$-BSA nanocomposite exhibits all the bands observed in the spectra of pure BSA and crosslinked BSA. The nanocomposite spectrum also has the characteristic band due to M–O stretching (400–580 cm^{-1}). The absorption due to M–OH and M–OH_2 (700–1100 cm^{-1}) stretching disappears and the band centred at 1075 cm^{-1} due to C–N stretching is much stronger than in the spectrum of pure BSA. These results indicate the occurrence of BSA interactions with the surface of the manganese ferrite nanoparticles. The FTIR findings clearly show modifications of oxide surface (M–OH and M–OH_2 stretching bands disappear) and the band centred at 1075 cm^{-1} is hypothesized to correspond to the interaction structure [21-23].

Figure 6 shows the XRD patterns of the $MnFe_2O_4$ nanoparticles, pure albumin and the composite material. The XRD pattern of the nanocomposite exhibits both amorphous BSA and nanocrystalline $MnFe_2O_4$ characteristics.

The organic content in the nanocomposite was obtained by analysing the C, H, N, content. In Table 3, results coming from elemental analysis data of the nanocomposite system are reported. As shown, the

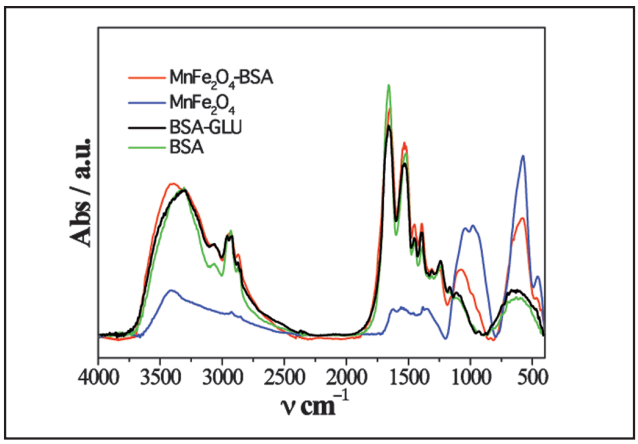

FIGURE 5 IR spectra of albumin (BSA), albumin cross-linked with glutaraldehyde (BSA-GLU), $MnFe_2O_4$ and $MnFe_2O_4$ entrapped in albumin cross-linked with glutaraldehyde ($MnFe_2O_4$-BSA)
Source: ENEA

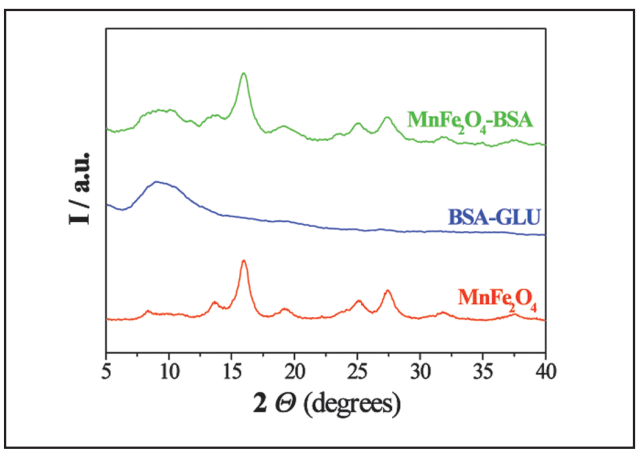

FIGURE 6 XRD patterns of albumin cross-linked with glutaraldehyde (BSA-GLU), $MnFe_2O_4$ and $MnFe_2O_4$ entrapped in albumin cross-linked with glutaraldehyde ($MnFe_2O_4$-BSA)
Source: ENEA

TABLE 3 Elemental analysis data of the nanocomposite system

Sample	Mass percentage (%)			BSA wt%	Glutaraldehyde cross-linked BSA wt%
	C	N	H		
BSA	47.3±0.3	14.4±0.1	7.2±0.1		
$MnFe_2O_4$ (C600)	<0.3	<0.1	<0.1		
$MnFe_2O_4$-BSA	32±3	7.8±0.6	4.9±0.4	53±5	61±5

Source: ENEA

obtained nanocomposite contains 61±5 %wt of albumin cross-linked with glutaraldehyde.

The morphology of the $MnFe_2O_4$-BSA nanocomposite was studied by a high resolution scanning electron microscope (HRSEM). In Figure 7 HRSEM images are shown. The composite particles (Figure 7, image B) are almost spherical in shape with average diameter of ~ 25 nm. The increase in particle size compared to $MnFe_2O_4$ nanocrystallites (d~5nm, Figure 7, image A) indicates that a polymer coating was obtained. Because of the extremely small dimensions of the

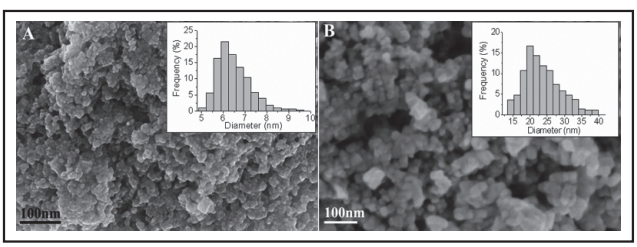

FIGURE 7 HRSEM images of (A) $MnFe_2O_4$ nanoparticles and (B) $MnFe_2O_4$-BSA composite
Source: ENEA

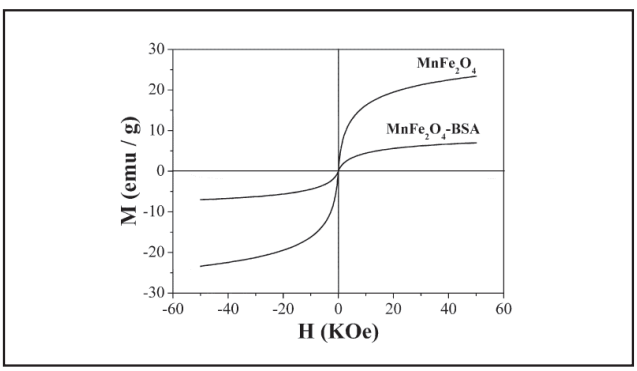

FIGURE 8 Field-dependent magnetization curves of manganese ferrite nanocrystals ($MnFe_2O_4$) and nanocomposite ($MnFe_2O_4$-BSA)
Source: ENEA

$MnFe_2O_4$ nanoparticles it is possible that several $MnFe_2O_4$ nanoparticles are coalesced into one $MnFe_2O_4$-BSA nanoparticle.

Since magnetic particles are dispersed in a non-magnetic matrix, it is important to investigate the influence of the carrier matrix on magnetism. Matrix-mediated particle agglomeration and magnetic interaction can greatly affect the overall properties of the system.

Field-dependent magnetizations for $MnFe_2O_4$ and $MnFe_2O_4$-BSA are shown in Figure 8. Performing the measurements at 300 K , the samples do not show a hysteresis loop, confirming a superparamagnetic behaviour. The encapsulation process does not influence the saturation magnetization of the manganese ferrite (*M*s = 9 emu g^{-1} at 300 K). The decrease in the magnetization value per gram of composite reflects the non-magnetic albumin content in the final material.

The third step of our work was the surface modification of the nanocomposite with drug adsorption.

The antibiotic was selected by considering both its antimicrobial spectrum of activity and its functional groups. In fact, this antibiotic possessed carboxyl groups able to establish ionic interactions with the amino groups of the nanoparticles.

The amount of adsorbed CEF in $MnFe_2O_4$-BSA was of (0.3±0.1) g_{CEF} /$g_{nanoparticles}$. Measuring bacterial growth in solution allowed to test the biological activity of the drug-functionalized particles. In Figure 9 the antibacterial activity of CEF-treated nanocomposite is shown. The bacterial growth remains at a controlled level for 2 days and subsequently increases. Although the drug release curve (shown in the inset of Figure 9) shows a short delivery time (*ca* 90% of the drug is released in 1 day), the low value of the minimum inhibitory concentration of CEF (0.2 gml^{-1}) against the tested strain of *S. epidermidis* guarantees the persistence of antibacterial activity.

The synthesized materials were tested *in vitro* with human larynx carcinoma. The information about cytoskeletal features is provided by fluorescence observations. Figure 10 shows representative fluorescent F-actin images of control cells after 24 h culture (Figure 10, image A) and of cells incubated with coated particles (Figure 10, image B). In all cases, cells exhibit well-organized stress fibres with defined cytoskeletal features. This response is a preliminary sign of no cell damage.

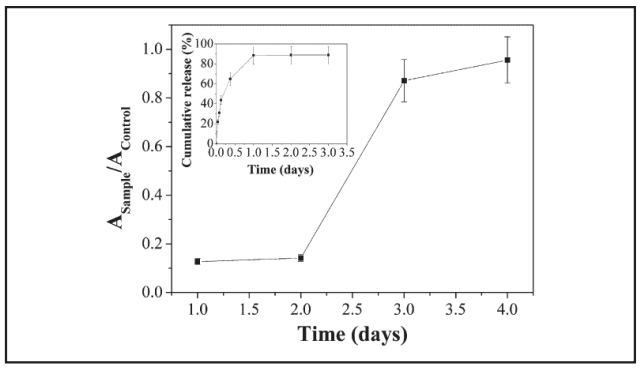

FIGURE 9 Normalized absorbance value of bacterial solutions in contact for increasing times with CEF-treated nanocomposite and of the control tube.
In the inset the cefamandole release from $MnFe_2O_4$-BSA nanocomposite is shown.
Source: ENEA

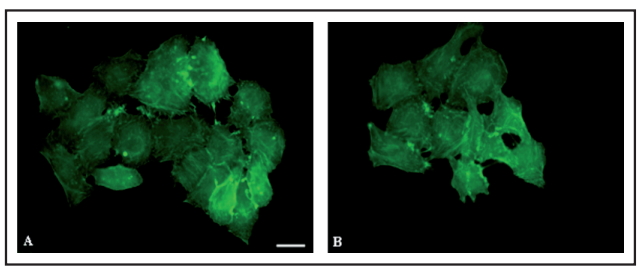

FIGURE 10 Fluorescence micrographs of Hp-2 cells stained for detection of F-actin Control cells (A); cells grown in presence of the nanocomposite for 24 h (B). Scale Bar = 10 µm.
Source: ENEA

Conclusion

In conclusion, we have developed a method to prepare superparamagnetic nanocomposite from albumin and magnetic nanoparticles. The optimized surfactant-assisted process and the preliminary adsorption of BSA on $MnFe_2O_4$ nanoparticles allowed the entrapment of high amount of ferrite into particles of BSA cross-linked with glutaraldehyde. The albumin, probably coordinating with surface metal-ions and surface hydroxyl groups of the ferrite, allows to efficiently stabilize ferrite nanoparticles in water phase and prevents their agglomeration.
To demonstrate that the obtained nanocomposite could potentially be used to deliver a selected drug, a model drug (cefamandole nafate) was ionically linked to the polymer. Delivery of cefamandole from these nanoparticles is rather rapid, but provides a release for at least 24h.
Deeper studies on the possibility to stabilize the produced systems in ferrofluid forms are underway; however the here reported preliminary results show that the developed nanobiotechnological particles possess physico-chemical characteristics interesting for biomedical applications.

References

[1] V.P. Torchilin (2000), *Drug targeting*, Eur. J. Pharm. Sci., 11, S81-S91.
[2] J.M. Collins (1984), *Pharmacologic rationale for regional drug delivery*, J. Clin. Oncol., 2, 498-504.
[3] P.K. Gupta and C.K. Hung (1990), *Comparative disposition of adriamycin delivered via magnetic albumin microspheres in presence and absence of magnetic field in rats*, Life Sci., 46, 471-84.
[4] P.K Gupta and C.K. Hung (1990), *Targeted delivery of low dose doxorubicin hydrochloride administered via magnetic albumin microspheres in rats*, J. Microencapsul., 7, 85-94.
[5] P.K. Gupta (1990), *Drug targeting in cancer chemotherapy: a clinical perspective*, J. Pharm. Sci., 79 949-962.
[6] Q.A. Pankhurst et al (2003), *Applications of magnetic nanoparticles in biomedicine*, J. Phys. D: Appl. Phys., 36, R167-181.
[7] Q.A. Pankhurst et al (2009), *Progress in applications of magnetic nanoparticles in biomedicine*, J. Phys. D: Appl. Phys., 42, 1-16.
[8] C. Alexiou et al. (2000), *Locoregional cancer treatment with magnetic drug targeting*, Cancer Research, 60, 6641-6648.
[9] S. Goodwin, C. Peterson, C. Hoh, C. Bittner, (1999), *Targeting and retention of magnetic targeted carriers (MTCs) enhancing intra-arterial chemotherapy*, J. Magn. Magn. Mater, 194, 132-139.
[10] A.S. Lubbe, C. Alexiou, C. Bergemann, (2001), *Clinical applications of magnetic drug targeting*, *J. Surg. Res.* 95, 200-206.
[11] A.S. Lubbe, C. Bergemann, J. Brock, D.G. McClure, (1999), *Physiological aspects in magnetic drug-targeting*, J. Magn. Magn. Mater. 194, 149-155.
[12] M. Bellusci, S. Canepari et al. (2007), *Phase evolution in synthesis of manganese ferrite nanoparticles*, J. of the Am. Ceram. Soc, 90, 3977-3983.
[13] M. Bellusci, A. La Barbera et al. (2009), *Preparation of albumin–ferrite superparamagnetic nanoparticles using reverse micelles*, Polymer International 58, 1142-1147.
[14] PCPDF-WIN version 2.01, November (1998) JCPDS-ICDD.
[15] A.A.Coelho, R.W. Cheary, (2007), *X-ray Line Profile Fitting Program* (XFIT), University of Technology, Sydney, Australia.
[16] H.M. Rietveld, (1967), *Line Profiles of Neutron Powder-Diffraction Peaks for Structure Refinement*', Acta Crystallogr., 22, 151-152 (a).; H.M. Rietveld, (1969), *A Profile Refinement Method for Nuclear and Magnetic Structures*, J. Appl. Crystallogr. 22, 65-71 (b).
[17] A.C. Larson and R.B. Von Dreele, (2004), *General Structure Analysis System* (GSAS). Los Alamos National Laboratory, Los Alamos, 86-748.
[18] ICSD Database, version 2004-02.
[19] V.M. Bujoreanu and E. Segal, (2001), *On the Dehydration of Mixed Oxides Powders Coprecipitated from Aqueous Solutions*, Solid State Sci., 3, 407-415.
[20] S. Okamoto, (1967), *Structure of the New d-Fe2O3 (Hydrate)*, J. Am. Ceram. Soc., 51, 594-598.
[21] V.M. Bujoreanu and E. Segal, (2002), *DSC Study of Water Elimination from the Coprecipitated Ferrite Powders*, J. Therm. Anal. Calorim., 68 191-197.
[22] M. Mikhaylova, D.K. Kim, C.C. Berry, A. Zagorodni, M. Toprak, A.S.G. Curtis et al. (2004), *BSA immobilization on amine-functionalized superparamagnetic iron oxide nanoparticles*, *Chem.* Mater., 16, 2344-2354.
[23] R.M. Silverstein, D. Kiemle and F.X. Webster, (2005), *Spectrometric Identification of Organic Compounds*, John Wiley & Sons, New York.